Magnetocaloric properties of $Mn_5(Si,P)B_2$ compounds for energy harvesting applications

Ojiyed, Hamutu; van den Berg, Maarten; Batashev, Ivan; Shen, Qi; van Dijk, Niels; Brück, Ekkes

DOI
10.1016/j.jallcom.2024.173485

Publication date
2024

Document Version
Final published version

Published in
Journal of Alloys and Compounds

Journal of Alloys and Compounds 978 (2024) 173485

Contents lists available at ScienceDirect

Journal of Alloys and Compounds

journal homepage: www.elsevier.com/locate/jalcom

Magnetocaloric properties of $Mn_5(Si,P)B_2$ compounds for energy harvesting applications

Hamutu Ojiyed, Maarten van den Berg, Ivan Batashev, Qi Shen, Niels van Dijk, Ekkes Brück *

Fundamental Aspects of Materials and Energy (FAME), Faculty of Applied Sciences, Delft University of Technology, Mekelweg 15, 2629JB Delft, the Netherlands

ARTICLE INFO

Keywords:
Magnetocaloric materials
Magnetocaloric effect
Second-order phase transition
Magnetocaloric energy harvesting
$Mn_5(Si,P)B_2$ compounds

ABSTRACT

The magnetocaloric properties of $Mn_5Si_{1-x}P_xB_2$ ($0 \leq x \leq 1$) compounds were studied for energy harvesting applications. The crystal structure and the magnetic structure were characterized by powder X-Ray Diffraction and powder Neutron Diffraction. The results indicate that these magnetocaloric materials crystallize in the tetragonal Cr_5B_3-type crystal structure. The introduction of P causes a stretching of the *c* axis and compression of the *a-b* plane, leading to a decrease in the unit-cell volume *V*. In the ferromagnetic state the magnetic moments align within the *a-b* plane, and the magnetic moment of the Mn1 atom on the 16 *l* site is larger than that of the Mn2 atom on the 4*c* site. The Curie temperature T_C can be adjusted continuously from 305 K ($x = 1$) to 406 K ($x = 0$) by replacing Si with P. The corresponding magnetic entropy change varies from 1.90 $Jkg^{-1}K^{-1}$ ($x = 0$) to 1.35 $Jkg^{-1}K^{-1}$ ($x = 1$) for a magnetic field change of 1 T. The PM-FM transition in these compounds corresponds to a second-order phase transition. $Mn_5Si_{1-x}P_xB_2$ compounds exhibit a magnetization difference of 28.1 - 31.3 Am^2kg^{-1} for a temperature span of 30 K around T_C in an applied magnetic field of 1 T. The considerable change in magnetization, the tunable T_C near and above room temperature and the absence of thermal hysteresis make these compounds promising candidates for magnetocaloric energy harvesting materials.

1. Introduction

There is a great deal of waste heat generated in modern industrial processes. The waste heat emitted by industrial processes is about 72% of all electrical energy produced worldwide in 2016 [1]. This industrial waste heat can partly be re-used if it is effectively utilized. In most cases the temperature of the produced industrial waste heat is only moderately higher than room temperature (300 - 400 K) [2]. Nevertheless, conventional thermoelectric generators are inefficient in this temperature range and expensive [3,4]. There have been several attempts to utilize the waste heat for energy harvesting. For example, magnetocaloric generators (or magnetocaloric motors) [5], shape memory alloy-based heat engines [6], as well as thermoacoustic engines [7] have been investigated. Among them, the magnetocaloric generator converts thermal energy into electrical energy by the difference in magnetization of soft magnetic materials at different temperatures. This energy harvesting concept was proposed by Nikola Tesla [8,9] as far back as the end of the 19th century. However, in order to use the concept efficiently it required the development of new magnetocaloric materials. Initially, magnetocaloric materials were studied for magnetic cooling applications, where the magnetic entropy change of the material induced by a change in applied magnetic field is converted into thermal energy [10–12]. It was later found that the inverse process in a power cycle could also be used for energy harvesting [13,14]. In recent years, the research of near room-temperature magnetocaloric materials (MCMs) has made great achievements, and many material systems have been explored: Gd and Gd alloys [15–19], Fe_2P-based [11,20–24], La$(Fe,Si)_{13}$ based [25,26], FeRh alloys [27,28] and Heusler alloys [29–31]. The research on these material systems is relatively mature, and each material system has its own advantages and disadvantages. Problems related to a poor mechanical stability or expensive raw materials often limit the applicability of the established MCMs. Finding new material systems that potentially meet the application requirements is therefore of interest.

The M_5XB_2 (M = Fe, Mn, Co, V, Cr and X = Si, P, S) materials system was previously studied for permanent magnet applications. In 1959 and 1960, Aronsson and Lundgren [32,33] reported that *M*-Si-B (M = Mn, Fe, Co) compounds could, under appropriate experimental conditions, crystallize in the tetragonal Cr_5B_3 crystal structure with *I4/mcm* symmetry (space group 140). Later, Rundqvist found that Fe-P-B alloys

* Corresponding author.
E-mail address: E.H.Bruck@tudelft.nl (E. Brück).

https://doi.org/10.1016/j.jallcom.2024.173485
Received 27 September 2023; Received in revised form 22 December 2023; Accepted 6 January 2024
Available online 10 January 2024

could also form in this structure [34]. The Curie temperatures of Fe_5SiB_2 and Fe_5PB_2 were reported to be 784 K [35] and 639 K [36], respectively. The high T_C values were the reason this system was considered as a potential permanent magnet material. In 2009, Almeida calculated the Curie temperature of Mn_5SiB_2 to be in the range of 469 - 492 K and found a saturation magnetization of 5.5 × 10^5 A/m [37]. Many studies on doping with 3*d* elements (Co, Cr, etc.) have been performed for (Mn, Fe)$_5$(Si,P)B_2 alloys [38–44]. Interestingly, Ericsson [45] and Cedervall [46] reported a spin reorientation around 170 K in Fe_5SiB_2, where the magnetic moment was oriented along the *c* axis at low temperatures and in the *a*-*b* plane above the spin reorientation temperature of 170 K. In 2010, Xie and coworkers [38] proposed that the Mn_5PB_2 compound had the potential to be used as a room-temperature MCM as the Curie temperature of 311 K is close to room temperature. Co-doped Fe_5PB_2 compounds are also a good candidates for room-temperature MCMs, as the Curie temperature of the Fe_5PB_2 compounds can be adjusted from 662 down to 152 K by the introduction of Co [43].

In this study, we investigated whether Mn$_5$(Si,P)B_2 compounds have the potential to be used as MCMs for energy harvesting applications. The Si/P ratio was adjusted over the full range, and the lattice structure was analyzed by X-Ray Diffraction (XRD) and Neutron Diffraction (ND) measurements. The magnetocaloric properties and magnetic structure were revealed by magnetic measurements and ND studies at low temperature. The results show that the Curie temperature of the compounds can be adjusted continuously in a wide temperature range above room temperature. A relatively high magnetization difference was found for a fixed temperature span around the magnetic transition. This makes them suitable for magnetocaloric energy harvesting applications that efficiently convert low-temperature waste heat into electricity.

2. Experimental details

The polycrystalline Mn_5SiB_2 compound was prepared by ball-milling the starting materials Mn (99.6% purity) , Si (99 +% purity) , B (99.4% purity) at a speed of 350 rpm for 10 h in a stainless steel jar with a sample-to-balls mass ratio of 1:4. The Mn_5PB_2 compound and the other compounds containing P were prepared with starting materials of MnP (96.08% purity), Mn (99.6% purity) and B (99.4% purity) powder by ball-milling at a speed of 350 rpm. The ball-milled samples were pressed into tablets with a diameter of 1 cm and a thickness of about 0.5 cm, and subsequently sealed in a quartz tube filled within 200 mbar of high-purity argon. The sealed samples were annealed in a furnace at 1150 °C for 24 h and then quenched in water. Room-temperature XRD was carried out with a PANalytical X-Pert PRO using Cu-K_α radiation. ND measurements were performed on the neutron powder diffractometer PEARL at the research reactor of the TU Delft [47]. Temperature-dependent XRD measurements were performed with an Anton Paar TTK450 temperature chamber. Differences in sample temperature and the control temperature were calibrated by comparing the Curie temperature obtained from XRD and SQUID magnetisation. Powder Neutron Diffraction data were collected at 80, 298 and 520 K using a fixed neutron wave length of λ = 1.665 Å. The samples were placed in a vanadium can with a diameter of 0.7 mm. The lattice structure and magnetic structure refinements were carried out using the Rietveld method [48] and the Fullprof software [49]. For the magnetic structure analysis in the ferromagnetic state we used the occupancies and internal coordinates obtained for the paramagnetic state at high temperatures. Magnetic measurements were carried out in a superconducting quantum interference device (SQUID) magnetometer (Quantum Design MPMS). Temperature-dependent magnetization was measured with a sweep rate of 2 K/min. The magnetic measurements at temperatures above 370 K and the heat capacity in a magnetic field of 1 T were performed in a VersaLab vibrating-sample magnetometer (VSM) with an oven function. The heat capacity measurements were carried out by Differential Scanning Calorimetry (DSC) measurements using a TA-Q2000 instrument (TA Instrument Company), equipped with a liquid nitrogen cooling system. The sweeping rate selected for the DSC measurements in this study was 10 K/min. Natural B is composed of 80% ^{11}B and 20% ^{10}B [50]. The absorption cross-section for thermal neutrons $\sigma_{a,th}$ at a neutron velocity of 2200 m/s for the ^{10}B isotope is as high as 3838 × 10^{-28} m^2, while for the ^{11}B isotope it corresponds to only 0.0055 × 10^{-28} m^2 [51]. This means that the presence of the ^{10}B isotope seriously affects the scattered intensity of the neutrons as a result of absorption. To avoid this effect, we used ^{11}B to re-prepare three samples $Mn_5Si^{11}B_2$, $Mn_5Si_{0.5}P^{11}_{0.5}B_2$ and $Mn_5P^{11}B_2$ for ND experiments using the same procedure as the previous parent sample (prepared with natural boron). The effect of crystallite orientation along an applied magnetic field in powder samples was studied by grinding the powder into small particles and then passing it through a 30 μm sieve. These powder samples were mixed with glue and placed in a magnetic field (of 1 T) for 24 h at room-temperature.

3. Results and discussion

3.1. The crystalline structures

XRD investigations conform that the $Mn_5Si_{1-x}P_xB_2$ ($0 \le x \le 1$) compounds all crystallize in the Cr_5B_3-type tetragonal structure with space group *I4/mcm*. Fig. 1(a) shows the XRD patterns taken at room temperature for the $Mn_5Si_{1-x}P_xB_2$ (x = 0.0, 0.6,0.8 and 1.0) compounds. For $0 \le x \le 0.5$ no additional diffraction peaks were observed besides the ones from the Mn_5SiB_2 main phase. However, a hexagonal Mn_2P impurity phase emerges for $x \ge 0.6$ and increases with the P content, as shown in Fig. 1(b). When Si is completely replaced by P (x = 1), the Mn_2P impurity phase reaches a weight fraction of 6.2 wt%. Fig. 1(c) and (d) show the lattice parameters *a* and *c*, the *c*/*a* ratio and the unit-cell volume *V* of the $Mn_5Si_{1-x}P_xB_2$ ($0 \le x \le 1$) main phase as a function of P content. The lattice parameters obtained by XRD were a = 5.61032(5) Å, c = 10.44349(9) Å for Mn_5SiB_2 (x = 0) and a = 5.53276(6) Å, c = 10.47474(12) Å for Mn_5PB_2 (x = 1), in good agreement with former studies [37,38]. Table 1 lists the lattice parameters and unit cell volume for the whole range of P-doping. The introduction of P reduced the unit-cell volume, as the atomic radius of P (0.98 Å) is slightly smaller than Si (1.11 Å). The change in the unit cell with P substitution is found to be anisotropic, as the changes in lattice parameters *a* and *c* have an opposite sign: the unit cell is stretched along the *c* axis, and compressed in the *a*-*b* plane. The effect of the lattice structure is important for the magnetic properties since it causes changes in the relative distances between the magnetic atoms and thus affects the magnetic coupling.

In Fig. 2(a) the XRD pattern for the ^{11}B containing sample $Mn_5P^{11}B_2$, which was prepared for the ND measurements, is shown. The $Mn_5P^{11}B_2$ compound also crystallized in Cr_5B_3-type structure (94.5 wt%) and is accompanied by a small amount of the Mn_2P impurity phase (5.5 wt%). Fig. 2(b) shows the lattice parameters of the main phase in $Mn_5Si_{1-x}P_xB_2$ (natural B) and in $Mn_5Si_{1-x}P^{11}_xB_2$ (with ^{11}B) for x = 0.0, 0.5 and 1.0. The XRD data at room temperature are almost identical. It can be seen that the introduction of ^{11}B has no significant effect on the formation of the main phase. The room-temperature (298 K) XRD and the high-temperature (520 K) and low-temperature (80 K) ND data show the same trend. The ND pattern for the $Mn_5P^{11}B_2$ compound in the paramagnetic state (T = 520 K) is shown in Fig. 2(c). The ND refinement confirms that this series of compounds crystallizes in the Cr_5B_3-type tetragonal structure, in good agreement with XRD results. We found that Mn occupies the 16 *l* and 4*c* sites, Si/P the 4*a* site and B the 8 *h* site (consistent with previous results). Häggström and coworkers [36] reported that part of the B occupies the 4*a* site in Fe_5PB_2. We did however not observe evidence for this in $Mn_5Si_{1-x}P^{11}_xB_2$ ($0 \le x \le 1$) compounds. The refined structural parameters from the ND measurements in the paramagnetic state are listed in Table 2.

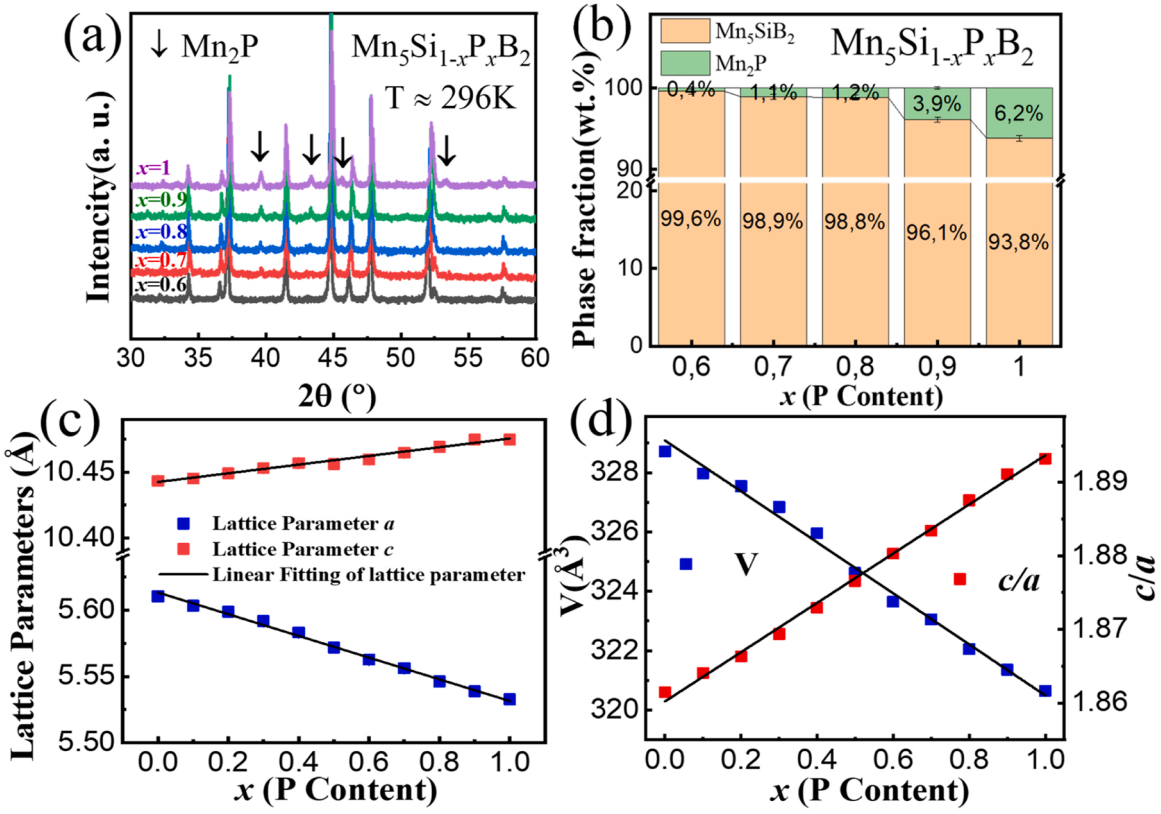

Fig. 1. (a) XRD patterns of $Mn_5Si_{1-x}P_xB_2$ (x = 0.0, 0.6,0.8 and 1.0) compounds. The peaks of the secondary Mn_2P phase are indicated by black arrows. (b) Weight fractions of the main and secondary phase for the $Mn_5Si_{1-x}P_xB_2$ (0.6 ≤x ≤1) compounds. (c) Lattice parameters of the main phase in the $Mn_5Si_{1-x}P_xB_2$ (0.6≤x≤1) compounds as a function of the P content. (d) Unit-cell volume and c/a ratio of the main phase in the $Mn_5Si_{1-x}P_xB_2$ (0 ≤x ≤1) compounds as a function of the P content.

Table 1
Lattice parameters a and c, unit-cell volume V, saturation magnetization M_S and ferromagnetic transition temperature T_C for the $Mn_5Si_{1-x}P_xB_2$ (0 ≤x ≤1) compounds. The lattice parameters and unit-cell volume were obtained by room-temperature XRD, M_s from SQUID magnetometer measurements at 5 K and T_C from SQUID magnetometer measurements in an applied field of 0.01 T.

x	a (Å)	c (Å)	V (Å^3)	M_s (Am^{2}kg^{-1})	(μ_B/f.u.)	T_C (K)
0.0	5.61032(4)	10.44349(9)	328.716(5)	105.56	6.13	406
0.1	5.60345(5)	10.44529(11)	327.968(5)	101.54	5.90	398
0.2	5.59878(4)	10.44915(9)	327.543(4)	105.16	6.12	386
0.3	5.59174(4)	10.45302(8)	326.840(4)	102.17	5.95	374
0.4	5.58316(4)	10.45688(9)	325.959(4)	101.16	5.90	359
0.5	5.57184(4)	10.45612(11)	324.614(5)	97.33	5.68	346
0.6	5.56262(5)	10.45959(11)	323.648(5)	100.43	5.86	339
0.7	5.55612(4)	10.46460(9)	323.047(4)	97.75	5.71	329
0.8	5.54635(4)	10.46912(8)	322.051(4)	99.25	5.81	318
0.9	5.53888(4)	10.47478(9)	321.358(4)	94.12	5.51	309
1.0	5.53276(6)	10.47474(12)	320.647(6)	91.07	5.34	305

3.2. Magnetocaloric effect

Fig. 3(a) shows the M-μ_0H curves measured at a temperature of 5 K. All magnetization curves show a typical soft ferromagnetic behavior without any magnetic hysteresis, where magnetic saturation is effectively reached at 1 T. Note, that a small high field susceptibility may be caused by local disorder. The saturation magnetization (M_s) of Mn_5SiB_2 and Mn_5PB_2 corresponds to 6.13 and 5.34 μ_B/f.u., respectively. The M_s value for all the $Mn_5Si_{1-x}P_xB_2$ ($0 \geq x \geq 1$) compounds is listed in Table 1. The average magnetic moment per manganese atom in Mn_5SiB_2 and Mn_5PB_2 is 1.37 and 1.12 μ_B/atom, respectively. Wäppling and coworkers [35] reported an average magnetic moment in Mn_5SiB_2 and Mn_5PB_2 of 1.6 and 1.1 μ_B/atom, respectively. The results for the Mn_5PB_2 compound are consistent, but Mn_5SiB_2 has a higher value in his report, which may be an overestimation since their calculation is based on NMR data. De Almeida and coworkers reported a magnetization for Mn_5SiB_2 that corresponds to 0.946 μ_B/atom at 300 K [37], which is slightly higher than our result of 0.882 μ_B/atom. The saturation magnetization of the $Mn_5Si_{1-x}P_xB_2$ compounds was found to depend on the Si/P ratio, as shown in Fig. 3(d). The introduction of P reduces the saturation magnetization.

Fig. 3(b) shows the temperature dependent magnetization (M-T) curves of Mn_5SiB_2 and Mn_5PB_2 for heating and cooling in an applied field of 1 T. The compounds show a ferromagnetic-to-paramagnetic phase transition near room temperature with a transition temperature T_C of 406 and 305 K, respectively. The transition temperature was

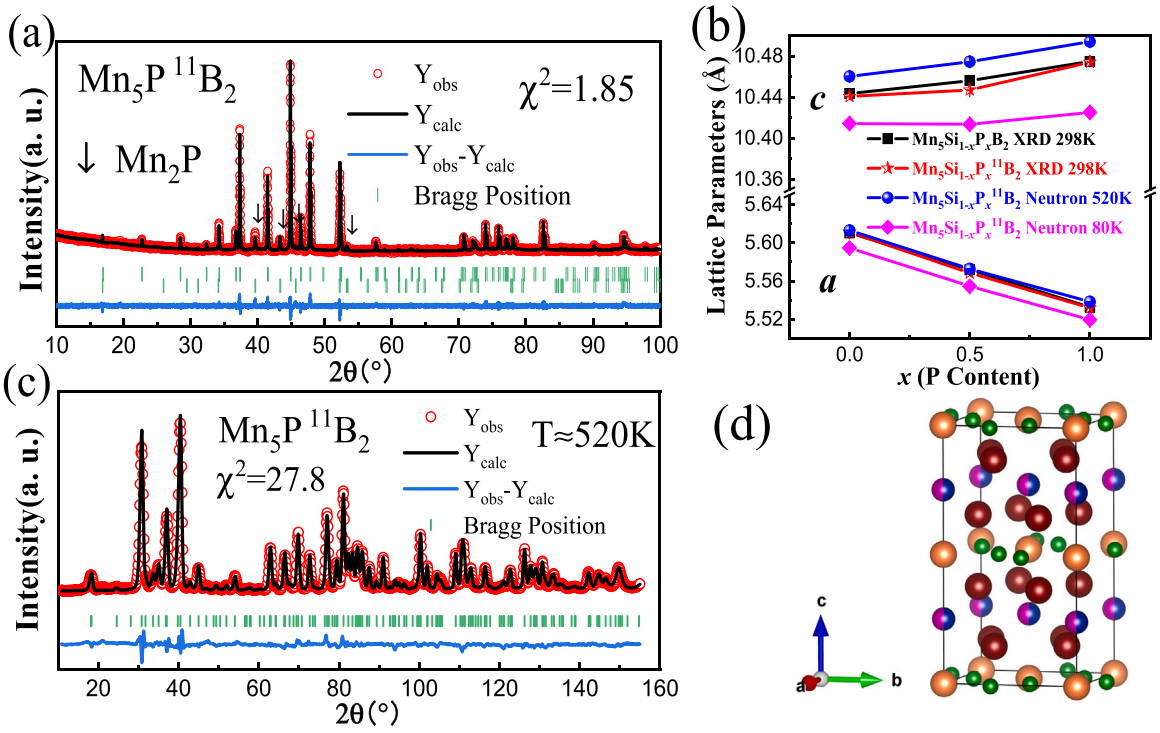

Fig. 2. (a) Room-temperature XRD pattern for the $Mn_5P^{11}B_2$ compound. The contribution from the Mn_2P phase is indicated by black arrows. (b) Lattice parameters of the main phase for $Mn_5Si_{1-x}P_xB_2$ ($x = 0$, $x = 0.5$ and $x = 1$) and $Mn_5Si_{1-x}P_x^{11}B_2$ ($x = 0$, $x = 0.5$ and $x = 1$) measured by XRD (at 298 K) and ND (at 80 and 520 K). (c) ND pattern of $Mn_5P^{11}B_2$ compound in the paramagnetic state ($T = 520$ K). (d) Crystal structure of $Mn_5(Si,P)B_2$. The different elements at the different sites are represented with dark brown for Mn at the 16 *l* site, light brown for Mn at the 4*c* site, purple/blue for Si/P at the 4*a* site and green for B at the 8 *h* site.

Table 2
Structural parameters of $Mn_5Si_{1-x}P_x^{11}B_2$ ($x = 0$, $x = 0.5$ and $x = 1$) in the paramagnetic state by ND. The numbers in parentheses are the refined errors. All the compounds crystallize in the Cr_5B_3-type structure with space group *I*4/*mcm* with Mn1 at the 16 *l* (x_1, x_1 +½, *z*) site, Mn2 at the 4*c* (0, 0, 0) site, P/Si at the 4*a* (0, 0, 1/4) site and B at the 8 *h* (x_2, x_2 +½, 0) Site.

	Parameters	$Mn_5Si^{11}B_2$	$Mn_5Si_{0.5}P_{0.5}^{11}B_2$	$Mn_5P^{11}B_2$
	a(Å)	5.61296(8)	5.57277(109)	5.53694(10)
	c(Å)	10.46029(9)	10.47449(402)	10.48970(37)
	V(Å^3)	329.555(11)	325.294(154)	321.590(14)
16 *l*	x_1	0.16719(14)	0.16840(209)	0.16950(19)
	z	0.13821(14)	0.13936(205)	0.14007(19)
8 *h*	x_2	0.61724(13)	0.61619(204)	0.61679(17)
4*a*	Occ(Si/P)	-	0.400(52)/0.600(52)	-
	R_P(%)	5.76	6.83	6.59
	R_{WP}(%)	7.62	10.4	9.19

obtained from the extreme value in the first derivative of the corresponding *M-T* curves in low magnetic field (0.01 T). These results are in good agreement with the values of 411 and 312 K previously reported by Wäppling and coworkers [35]. Xie and coworkers [38] reported a slightly lower value of 302 K for Mn_5PB_2. Heating and cooling *M-T* curves coincide without thermal hysteresis, suggesting that these compounds show a second-order phase transition (SOPT) at T_C. The *M-T* curves in a field of 1 T and the first derivatives of the *M-T* curves in a field of 0.01 T are shown in Fig. 3(c). The value of T_C shows a strong dependence on the Si/P ratio and decreased with P content. An increase in P content of 10 at% causes a decrease in T_C of about 10 K, resulting in $dT_C/dx \approx 1$ K/at%. The T_C values of the $Mn_5Si_{1-x}P_xB_2$ ($0 \geq x \geq 1$) compounds are listed in Table 1. The results are similar to those observed by Wäppling *et al.* [35] and Häggström *et al.* [36] for Fe_5SiB_2 - Fe_5PB_2 compounds. Fig. 3(d) shows T_C as a function of the P content, indicating that T_C in the $Mn_5Si_{1-x}P_xB_2$ ($0 \leq x \leq 1$) compounds can be varied continuously in the temperature range from 305 to 406 K by adjusted the Si/P ratio. This fulfills one important application requirements of MCMs that the transition temperature can be adjusted continuously over the temperature range of interest for the application.

For the magnetocaloric energy harvesting cycle low-grade waste heat Q_{in} is used as an energy source, and the magnetization difference caused by the material after being heated by it will cause the change of Gibbs free energy: $E_M = -\mu_0 \Delta MH$, and then convert it into kinetic or electrical energy, where the $\Delta M = M_{cold} - M_{hot}$ is the magnetization difference between the two temperature reference temperatures above (T_{hot}) and below (T_{cold}) the phase transition temperature (T_C). A key property for magnetic energy harvesting materials is the thermodynamic efficiency $\eta = -\mu_0 \Delta MH/Q_{in}$, defined by the ratio of the upper-limit magnetic energy E_M and the required heat Q_{in} [13]. In Fig. 4, we show the *M-T* and C_p-*T* curves in the vicinity of the transition temperature for the $Mn_5Si_{0.5}P_{0.5}B_2$ compounds and the ΔM and Q_{in} values for a temperature span ΔT of 30 K symmetrically placed around T_C. According to a study by Dzekan and coworkers [52], FOPT materials generally have a relatively high ΔM, but due to the presence of latent heat, the required input heat energy Q_{in} is also significant, which in turn reduces its efficiency. Although the ΔM of the SOPT materials are generally smaller than the ΔM of FOPT materials, the absence of thermal hysteresis and the smaller Q_{in} make them competitive. In our study, ΔM for Mn_5PB_2 and $Mn_5Si_{0.5}P_{0.5}B_2$ compounds are 28.1 and 31.1 Am^{2}kg^{-1}, respectively. The ΔM of these two compounds is comparable to those for Heusler alloys, as reported by Dzekan and coworkers [52]. The ΔM values for Mn_5PB_2 and $Mn_5Si_{0.5}P_{0.5}B_2$ compounds are higher than the majority of the reported Heusler alloys. The Q_{in} values for the Mn_5PB_2 and $Mn_5Si_{0.5}P_{0.5}B_2$ compounds correspond to 18.8 and 20.9 J/kgK, respectively. The value of ΔM and Q_{in} for the $Mn_5Si_{1-x}P_xB_2$ ($x = 0.0$, 0.5 and 1.0) compounds are shown in Table 3.

The specific heat capacity as a function of temperature for the $Mn_5Si_{1-x}P_xB_2$ ($x = 0.0$, 0.2, 0.4, 0.6, 0.8 and 1.0) compounds is shown in Fig. 5(a). A discontinuous step in the specific heat capacity is observed at the transition temperature, which is characteristic for a SOPT. We

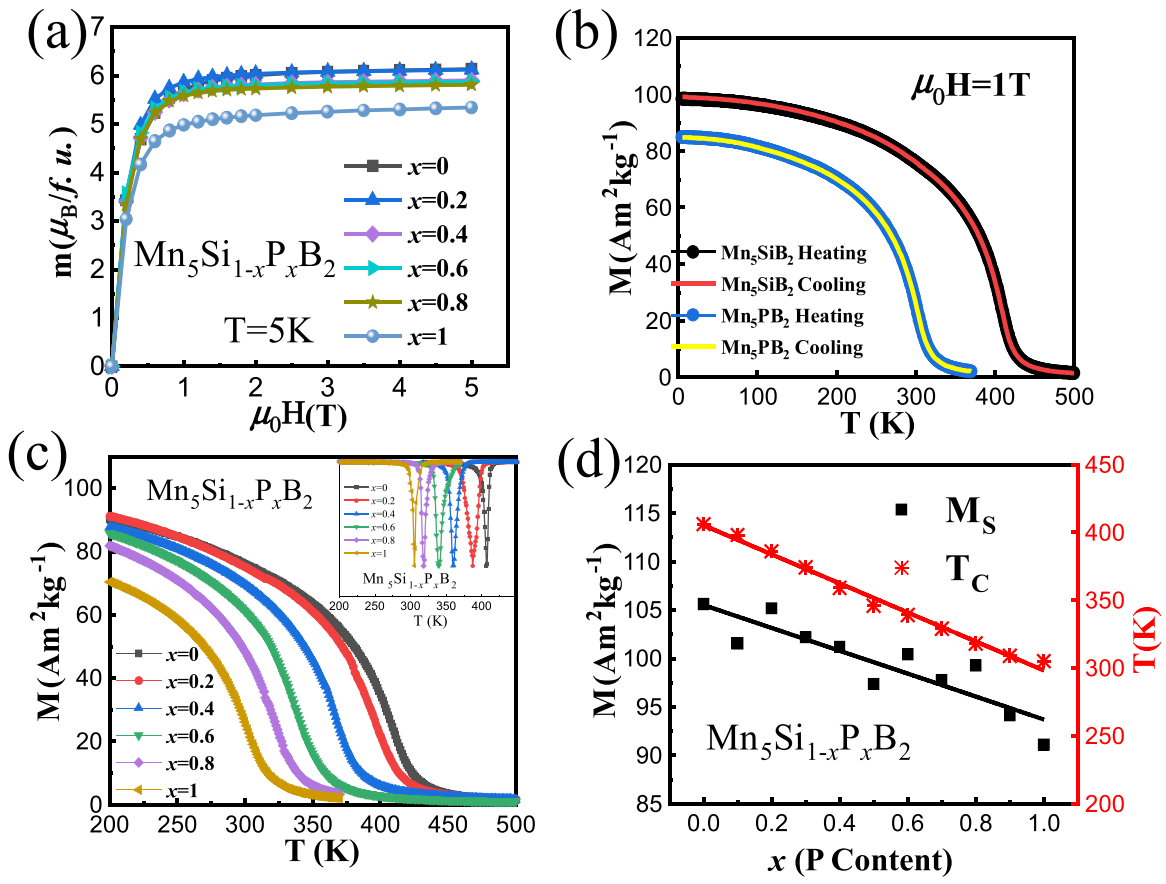

Fig. 3. (a) Field-dependent magnetization of the $Mn_5Si_{1-x}P_xB_2$ ($x = 0.0$, 0.2, 0.4, 0.6, 0.8 and 1.0) compounds measured at 5 K. (b) Temperature-dependent magnetization of the Mn_5SiB_2 and Mn_5PB_2compounds in a field of 1 T for heating and cooling. (c) Temperature-dependent magnetization of the $Mn_5Si_{1-x}P_xB_2$ ($x = 0.0$, 0.2, 0.4, 0.6, 0.8 and 1.0) compounds. The inset shows the reduced first derivative of the low-field *M-T* curve in a field of 0.01 T. (d) Values of T_C (red) and M_S (black) for $Mn_5Si_{1-x}P_xB_2$ ($0 \geq x \geq 1$) as a function of the P content *x*.

calculated the isothermal magnetic entropy change of the compounds from the *M-T* data at different magnetic field changes (0.05–2 T) using equation $\Delta S_M(T)_{\Delta H} = \int_{Hi}^{H_f} \mu_0 \left(\frac{\partial M(T,H)}{\partial T}\right)_H dH$ [15]. The estimated isothermal magnetic entropy change is shown in Fig. 5(b) for a field change of $\mu_0 \Delta H = 1$ T (for a field between 0 and 1 T). The transition temperature moves to lower temperatures for an increase in P content. The corresponding maximum $|\Delta S_M|$ for Mn_5SiB_2, $Mn_5Si_{0.5}P_{0.5}B_2$ and Mn_5PB_2 in a field change of 1 T is 1.90, 1.33 and 1.35 $Jkg^{-1}K^{-1}$, respectively. For comparison, the isothermal magnetic entropy curve of Gd is also shown in Fig. 5(b). The maximum value of $|\Delta S_M|$ for our sample is slightly lower than the value of 2.46 $Jkg^{-1}K^{-1}$ of Gd. The maximum magnetic entropy change $|\Delta S_{M,\ max}|$ for $Mn_5Si_{1-x}P_xB_2$ ($x = 0.0$, 0.5 and 1.0) compounds are listed in Table 3.

The *M-T* and DSC curves of these compounds show typical SOPT characteristics. Law and coworkers [54] proposed a quantitative analysis to evaluate the nature of the phase transition. The magnetic entropy change is proposed to scale as a power law with the magnetic field $|\Delta Sm| \propto H^n$, where the exponential $n = \frac{d\ln(|\Delta Sm|)}{d\ln(H)}$ will demonstrate a sharp change near the transition temperature. Using the Bean and Rodbell model [55] it was demonstrated that it can distinguish whether a material shows a FOPT or a SOPT by evaluating the field exponent *n* across the phase transition. For materials with a FOPT, the maximum value of the field exponent n_{max} is greater than 2, while it remains equal or less than 2 for a SOPT (this is also the case for the critical point between the FOPT and the SOPT). Moreover, the minimum value for the field exponent n_{min} is also characteristic for the transition where $n_{min} = 2/3$ for the SOPT, $n_{min} = 2/5$ for the critical point between the FOPT and the SOPT and $n_{min} < 2/5$ for the FOPT. Van Dijk [56] later demonstrated that these predictions are also found when the Landau model [57] is applied to describe the phase transition. Fig. 5(c) shows the temperature dependence of the field exponent *n* for the $Mn_5Si_{1-x}P_xB_2$ ($x = 0.0$, 0.5 and 1.0) compounds. The maximum value for the field exponent does not exceed the value of 2 in the vicinity of the phase transition. The minimum value for the field exponent n_{min} is very similar for all three compounds and reaches a value slightly above 2/3. All these observations confirm that these three materials show a SOPT.

Temperature-dependent XRD was used to characterize the magneto-elastic coupling in the Mn_5SiB_2 compound. Fig. 6(a) shows the unit-cell volume as a function of temperature for Mn_5SiB_2 in the temperature range from 298 to 429 K. Interestingly, the volume of the unit cell reduces with temperature in a narrow temperature range (360 - 400 K) below T_C. In this temperature range a weak negative thermal expansion (NTE) is observed, which originates from the temperature-dependent magneto-elastic coupling. In the low-temperature range (well below T_C), all the magnetic moments are well aligned along the easy direction, and the magnetic moments deviate from the easy direction, while with the increase in temperature the magnetic order gradually collapses when the temperature approaches T_C. As the magneto-elastic coupling scales with the magnetic order, the lattice may experience a negative thermal expansion in case the magnetic order weakens when T_C is approached. Above the ferromagnetic transition temperature, the magnetic order vanishes, and thereby also the magneto-elastic coupling, resulting in the conventional thermal expansion of the paramagnetic state V_{PM} [58,59]. In Fig. 6(a) the magneto-elastic contribution in the magnetically ordered state is estimated from the extrapolated temperature dependence of the unit-cell volume of the paramagnetic state. The difference ΔV between the experimental data V_{exp} of the ferromagnetic

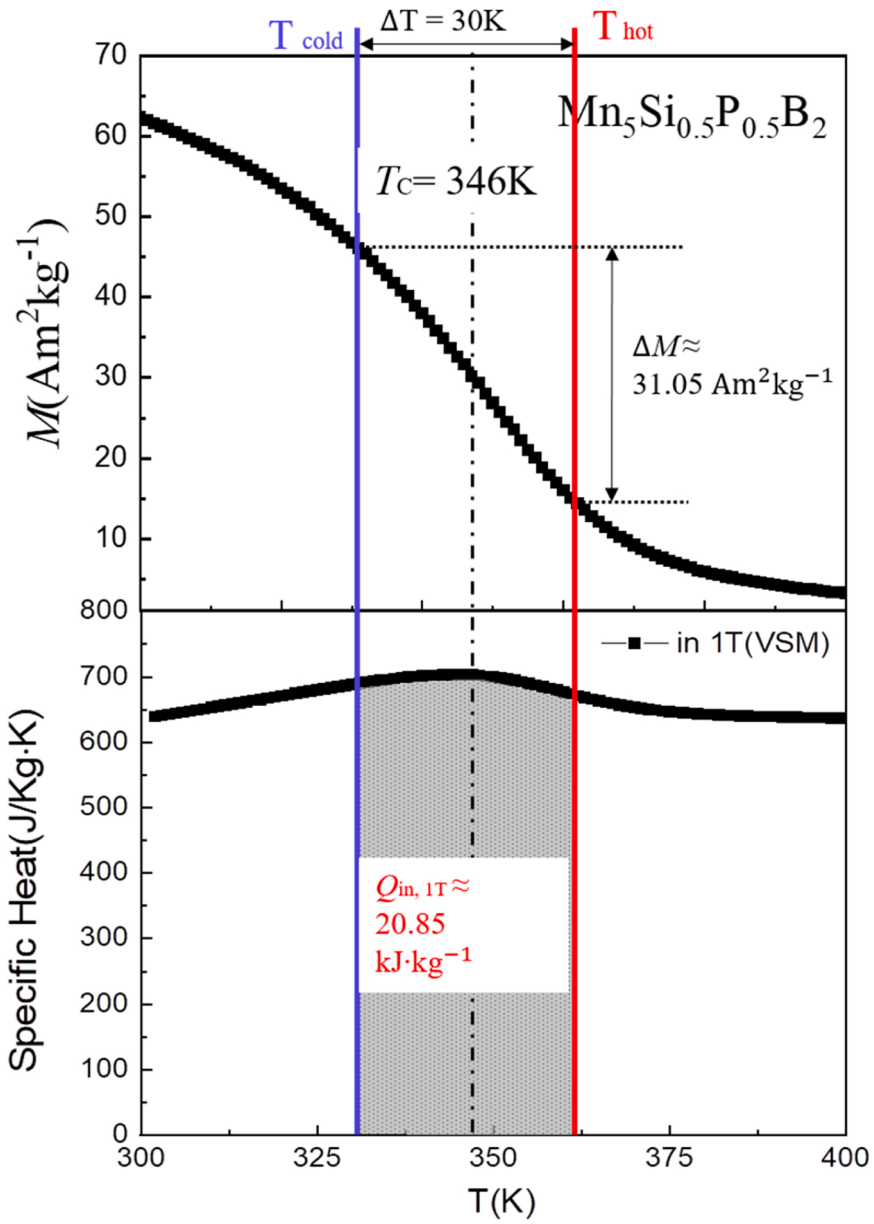

Fig. 4. (a) *M-T* curve of $Mn_5Si_{1-x}P_xB_2$ compound near the Curie temperature in a magnetic field of 1 T, where ΔM is the difference in magnetization for a temperature span of $\Delta T = T_{hot}$ - $T_{cold} = 30$ K. (b) Temperature dependence of the heat capacity. The heat input Q_{in} is defined by the integral of the heat capacity measured in 1 T over the temperature span of $\Delta T = 30$ K.

Table 3
Calculated $|\Delta S_{M,\,max}|$ and ΔM and Q_{in} ($\Delta T = 30$ K) for $Mn_5Si_{1-x}P_xB_2$ ($x = 0.0$, 0.5 and 1.0) in 1 and 2 T, data for Gd from literatures [52,53] and Gd in this work are shown as a comparison.

	Applied field	Gd (in this work)	Gd	$Mn_5Si\ B_2$	$Mn_5Si_{0.5}P_{0.5}B_2$	Mn_5PB_2
$\Delta S_{M,max}$ ($Jkg^{-1}K^{-1}$)	0-1 T	2.46	2.8[53]	1.90	1.33	1.35
	0-2 T	3.69	—	3.16	2.36	2.26
ΔM (Am^2kg^{-1})	1 T	63.4	77[52]	—	31.05	28.12
Q_{in} ($kJkg^{-1}$)	1 T	—	19.2[52]	—	20.85	18.88

state and the extrapolated paramagnetic state V_{PM} can be regarded as the contribution from the magneto-elastic coupling. The gradual variation in the unit-cell volume as a function of the temperature near T_C between 400 and 410 K, is expected to reflect the short-range order in the paramagnetic state (just above T_C). It is interesting to note that the NTE is strongly anisotropic. As shown in Fig. 6(b) the negative thermal expansion is only observed within the *a*-*b* plane (*a* axis) and not along the *c* axis. This is related to the magnetic structure of the compound, which we will discuss in the next section.

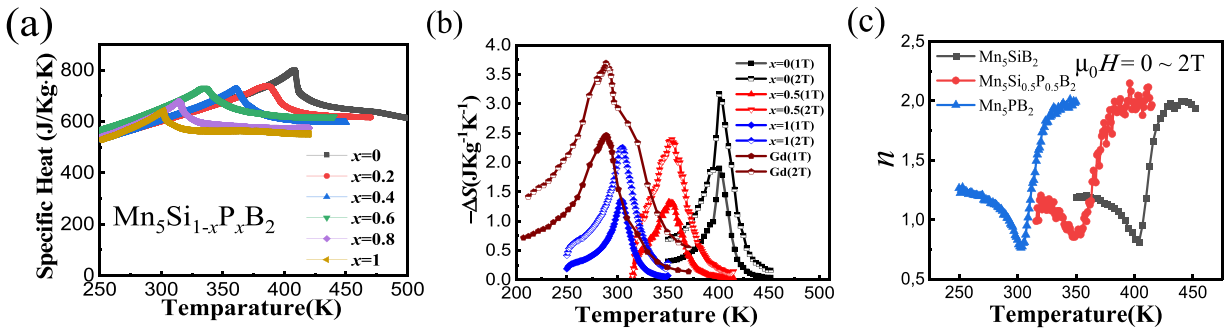

Fig. 5. (a) Temperature dependence of the specific heat capacity of the $Mn_5Si_{1-x}P_xB_2$ ($x = 0.0$, 0.2, 0.4, 0.6, 0.8 and 1.0) compounds. (b) Magnetic entropy change $-\Delta S_M$ as a function of temperature for a field change of 1 and 2 T. The data for Gd have been added as reference. (c) Field exponent of the magnetic entropy change $n = \frac{d\ln(|\Delta Sm|)}{d\ln(H)}$ for the $Mn_5Si_{1-x}P_xB_2$ ($x = 0.0$, 0.5 and 1.0) compounds.

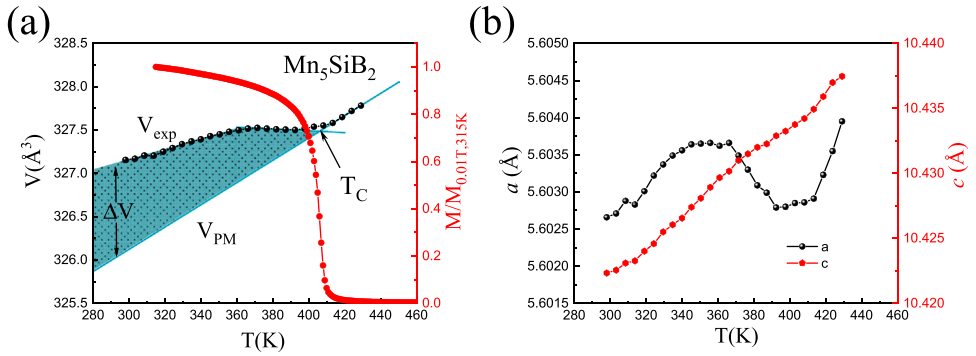

Fig. 6. (a) Temperature dependence of the unit-cell volume V and the normalized M-T curve in a magnetic field of 0.01 T for the Mn_5SiB_2 compound. The ferromagnetic transition temperature T_C is indicated by the arrow. (b) Temperature dependence of the lattice parameters a and c for the tetragonal Mn_5SiB_2 compound.

3.3. Magnetic structure

Magnetic anisotropy of the materials is also an important factor for magnetocaloric applications, especially for the magnetocaloric generators. As polycrystalline soft magnetic materials are used in generators, a low magnetic anisotropy means the materials can be magnetized more easily in relatively low magnetic fields, resulting in a larger magnetization difference for a given temperature span. To determine the magnetic structure of the $Mn_5Si_{1-x}P_xB_2$ ($0 \leq x \leq 1$) compounds, ND was carried out in both the ferromagnetic and the paramagnetic state. For the neutron powder diffraction samples containing the ^{11}B isotope (instead of natural B) were prepared with composition $Mn_5Si_{1-x}P_x^{11}B_2$ ($x = 0.0$, 0.5 and 1.0). It is necessary to ensure that the $Mn_5Si_{1-x}P_x^{11}B_2$ compounds have the same lattice structure and magnetic properties as the corresponding mother compounds prepared with natural boron. In the phase analysis section we have discussed that the ^{11}B samples have the same lattice structure as the mother compounds. For the M-μ_0H curves in Fig. 7(a) and the M-T curves in Fig. 7(b), the ^{11}B compounds shows almost the same characteristics as the natural B containing mother compounds. This means we can confidently use ^{11}B compounds as representative for the magnetic structure in the mother compounds. Fig. 8(a) shows the ND pattern of the $Mn_5Si^{11}B_2$ compound in both the FM state (80 K) and the PM state (520 K). Due to the magnetic form factor $f(\mathbf{Q})$ the magnetic scattering (proportional to $|f(\mathbf{Q})|^2$) rapidly attenuates for increasing scattering angles. This means that the peaks in the low-angle scattering range provide most reliable information regarding the magnetic structure in the FM state. We didn't observe any new peaks in the FM state compared to the PM state, indicating that the

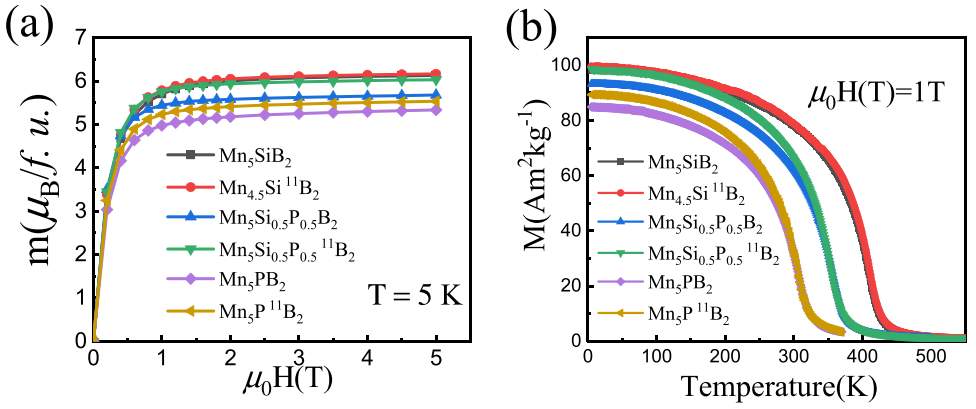

Fig. 7. (a) Field-dependent magnetization of the $Mn_5Si_{1-x}P_xB_2$ and $Mn_5Si_{1-x}P_x^{11}B_2$ ($x = 0.0$, 0.5 and 1.0) compounds at a temperature of 5 K. (b) Temperature-dependent magnetization of the $Mn_5Si_{1-x}P_xB_2$ and $Mn_5Si_{1-x}P_x^{11}B_2$ ($x = 0.0$, 0.5 and 1.0) compounds in an applied field of 1 T.

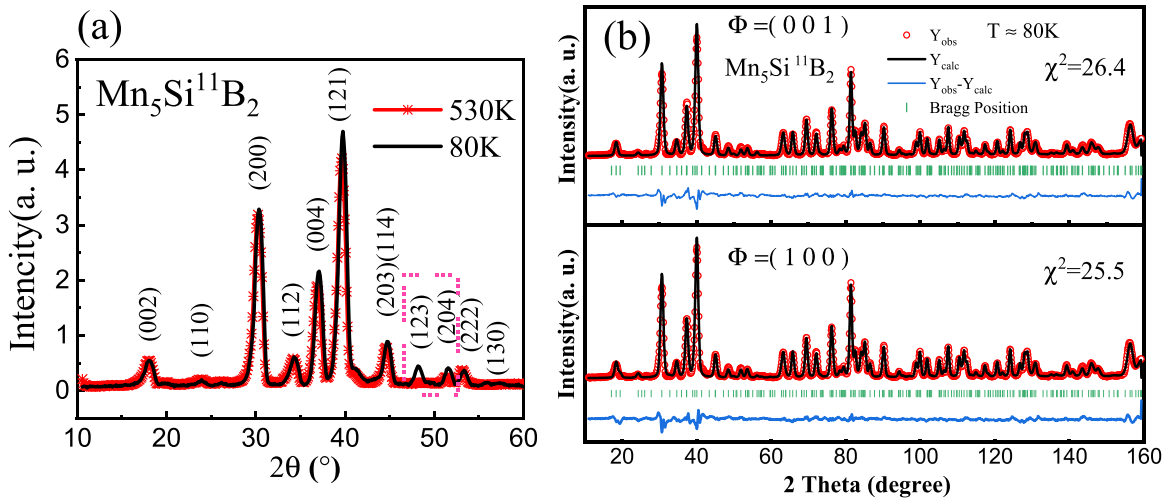

Fig. 8. (a) Neutron diffraction patterns for the $Mn_5Si^{11}B_2$ compound in the ferromagnetic state (80 K) and in the paramagnetic state (520 K). (b) Comparison of the neutron powder diffraction refinements for the $Mn_5Si^{11}B_2$ compound in the ferromagnetic state using different basis functions, with Φ = (001) at the top and Φ = (100) at the bottom.

size of the magnetic unit cell is the same as the nuclear unit cell. This means that the propagation vector for the magnetic structure corresponds to **k** = (0,0,0). The most obvious difference between the neutron diffraction patterns of the FM and PM state is the increase in intensity for the (213) and (204) peaks in the FM state, reflecting a relatively strong magnetic contribution.

A representational analysis of space group 140 (tetragonal *I4/mcm* symmetry) has been performed with the SARAh software package [60]. Table 4 shows the possible irreducible representations and the corresponding basis vectors for the magnetic structure in space group 140. According to a previous report [35,46], this system has two magnetic sites for the Mn atoms: Mn1 at the 16 *l* site and Mn2 at the 4*c* site. As we observe a single magnetic transition in the DSC and SQUID magnetization measurements, the two magnetic sites are strongly coupled and must be represented by the same irreducible representations, namely Γ1, Γ3 and Γ9. The Γ1 representation is an antiferromagnetic ordering, while our samples show typical ferromagnetic order characteristics in magnetic measurements, so it can be excluded. The Γ3 representation has its basis vector along the *c* axis for the two magnetic sites, and the Γ9 representation has its basis vector aligned within the *a*-*b* plane. We used the Γ3 and Γ9 representations to refine the ND data and found that the quality of fit in the refinement was relatively close for these two models, as shown in Fig. 8(b). This makes it difficult to conclude what orientation the magnetic moments have.

In order to determine the direction of its magnetic moment, the Mn_5SiB_2 powder was oriented in a magnetic field at room temperature. Fig. 9(a) shows a comparison between the XRD pattern of the field-oriented powder and the free powder sample. The (004) and (006) peaks, which have a plane normal along the *c* axis in the oriented sample, all disappear. On the other hand, the (110), (200) and (220) peaks, which have a plane normal in the *a*-*b* plane, are all significantly enhanced. Therefore, we can conclude that in the FM state at room-temperature the magnetic moments are oriented within the *a*-*b* plane. Based on the tetragonal *I4/mcm* symmetry of space group 140, there are two possible orientations within the *a*-*b* plane, namely: (100) or (110).

According to the calculated contribution of the magnetic scattering to the ND pattern in Fig. 9(b), it is concluded that low-angle diffraction peaks of the (002) and (101) crystal planes will be observed if the magnetic moments are aligned along the (110) direction, this is not the case in our result, no magnetic contribution is observed on these two peaks (see Fig. 8(a)). We therefore conclude that the magnetic moments are oriented along the (100) direction.

This result also explains the observed anisotropy in the negative thermal expansion. As the magnetic moments are arranged in the *a*-*b* plane, the effect of the magnetic moment on the thermal expansion is much larger in this direction than along the *c* axis. Fig. 9(c) shows the obtained magnetic structure of Mn_5SiB_2.

Fig. 10(a) shows the total magnetic moment per formula unit obtained by ND refinement and SQUID magnetization for the $Mn_5Si_{1-x}P_x^{11}B_2$ (x = 0.0, 0.5 and 1.0) compounds. The total magnetic moment decreases with increasing P content. It is worth noting that the values from the ND data are higher than those from the SQUID data. To check this Fig. 10(b) shows a plot of M as a function of $1/\mu_0 H$. From this plot the saturation magnetization can be estimated by a linear fit of the curve. In order to avoid the effect of demagnetizing fields, only the data above 1 T were used. The saturation magnetization obtained by fitting in Fig. 10(a) is slightly higher than those of the SQUID magnetization data in 5 T, but still slightly lower than the magnetization obtained by ND. Fig. 10(c) shows the individual magnetic Mn moments for the two inequivalent positions (Mn1 at the 16 *l* site and Mn2 at the 4*c* site) obtained by ND. The magnetic moment of Mn is larger at the 16 *l* site than at the 4*c* site, consistent with the reported result for Mn_5SiB_2 by Wäppling and coworkers [35]. The introduction of P has a different effect on the two magnetic moments: the moment on the 16 *l* site decreases with P content, while the moment on the 4*c* site remains more or less constant with increasing P content.

Table 4
Representational analysis results for space group 140 (tetragonal *I4/mcm* symmetry) with propagation vector **k** = (0,0,0) and two magnetic sites at 16*l* and 4*c* given by SARAh. For each magnetic site, the possible magnetic ordering was given: antiferromagnetic (AFM) or ferromagnetic (FM), and the number of basis vectors Φ_i.

Irreducible Representation	Magnetic 16*l* site		Magnetic 4*c* site	
	Φ in *a*-*b* plane	Φ in *c* axis	Φ in *a*-*b* plane	Φ in *c* axis
Γ_1	1 (AFM)	0	0	1 (AFM)
Γ_2	1 (AFM)	1 (AFM)	0	0
Γ_3	1 (AFM)	1 (FM)	0	1 (FM)
Γ_4	1 (AFM)	0	0	0
Γ_5	1 (AFM)	1 (AFM)	0	0
Γ_6	1 (AFM)	0	0	0
Γ_7	1 (AFM)	0	0	0
Γ_8	1 (AFM)	1 (AFM)	0	0
Γ_9	2 (FM) 4 (AFM)	0	2 (FM) 4 (AFM)	0
Γ_{10}	4 (AFM)	2 (FM)	0	0

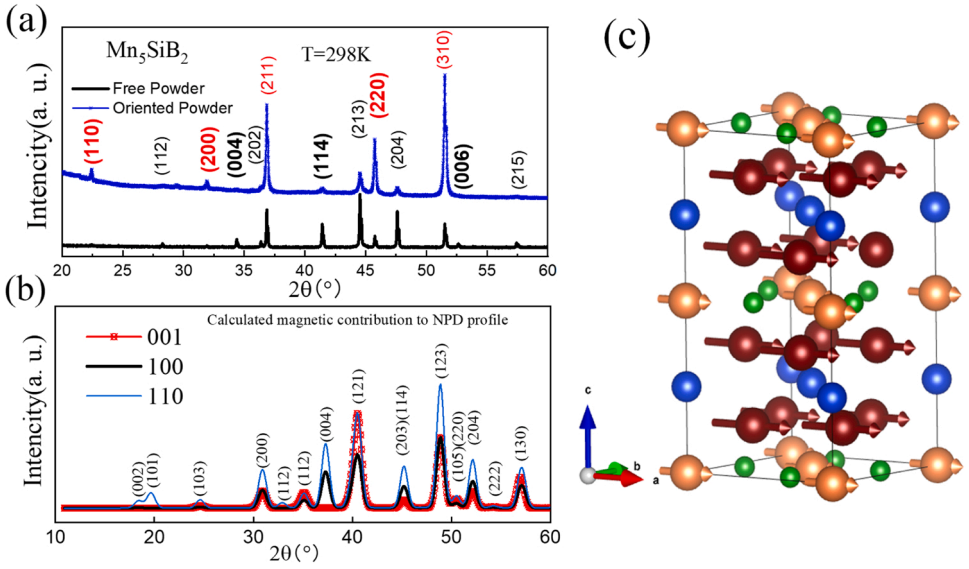

Fig. 9. (a) Field-oriented powder and free powder XRD patterns of the Mn_5SiB_2 compound in the ferromagnetic state at room temperature (298 K). (b) The comparison of the calculated magnetic contributions for three different magnetic moment directions in free powder ND: Φ = (001), (100) and (110). (c) Magnetic structure of the $Mn_5Si^{11}B_2$ compound in the ferromagnetic state. The length of arrow corresponds to the size of the magnetic moment.

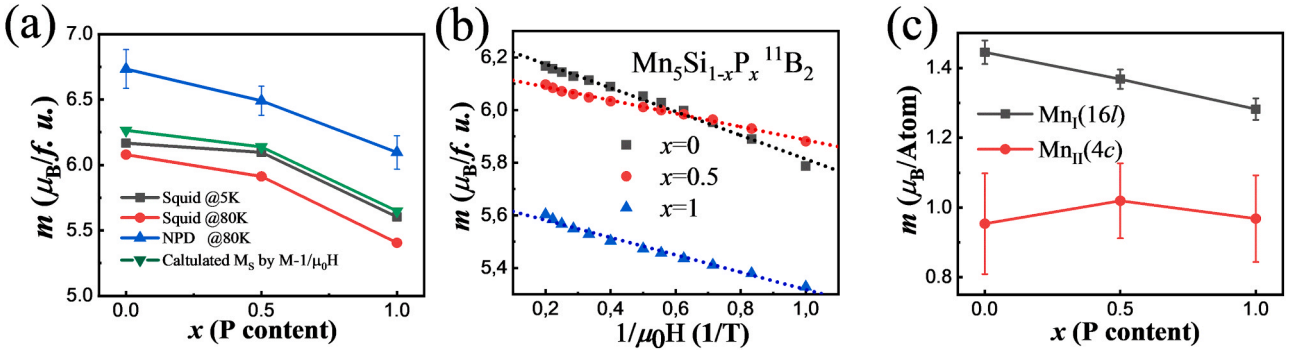

Fig. 10. (a) Saturation magnetization of the $Mn_5Si_{1-x}P_x^{11}B_2$ compounds (x = 0.0, 0.5 and 1.0) obtained by neutron diffraction and SQUID magnetization at different temperatures. (b) Magnetization versus $1/\mu_0 H$ curve for the $Mn_5Si_{1-x}P_x^{11}B_2$ compounds (x = 0.0, 0.5 and 1.0). (c) Magnetic moments for Mn1 at the 16 *l* site and Mn2 at the 4*c* site in the tetragonal lattice of the $Mn_5Si_{1-x}P_x^{11}B_2$ compounds (x = 0.0, 0.5 and 1.0).

4. Conclusions

The magnetocaloric properties, lattice and magnetic structure of the $Mn_5Si_{1-x}P_xB_2$ compounds have been studied in the whole range of P substitution ($0 \leq x \leq 1$). All compounds crystallize in the tetragonal Cr_5B_3-type structure (*I*4/*mcm* symmetry), where the P atom replaces the Si at the 4*c* site in the unit cell, which leads to a decrease in the unit-cell volume. The $Mn_5Si_{1-x}P_xB_2$ ($0.6 \leq x \leq 1.0$) compounds are accompanied by a small amount of Mn_2P impurity phase, 6.2 wt% for $x = 1.0$. As a result of a significant magneto-elastic coupling in the ferromagnetic state, Mn_5SiB_2 exhibits a negative thermal expansion between 360 and 400 K. The neutron diffraction results reveal that the compounds show FM ordering with moments on the Mn atoms oriented within the *a*-*b* plane below the ferromagnetic transition temperature. Although the P doping reduces M_s, the compounds still exhibit a considerable ΔM up to 31.25 Am^2kg^{-1} for $\Delta T = 30$ K in a applied magnetic field of 1 T. The value of T_C can continuously be adjusted in the near room-temperature range between 305 and 406 K by the Si/P ratio. Although the compounds are not competitive for magnetic cooling due to their lower value of $|\Delta S_M|$ (1.35 to 1.90 $Jkg^{-1}K^{-1}$ in a field change of 1 T), the considerable ΔM and the continuously adjustable T_C in the temperature range above room temperature makes them promising candidate materials for magnetocaloric energy harvesting applications.

CRediT authorship contribution statement

Brück Ekkes: Supervision, Writing – review & editing. **van Dijk Niels:** Supervision, Writing – review & editing. **Shen Qi:** Data curation. **Batashev Ivan:** Data curation, Investigation. **van den Berg Maarten:** Data curation, Formal analysis. **Ojiyed Hamutu:** Writing – original draft.

Declaration of Competing Interest

The authors declare the following financial interests/personal relationships which may be considered as potential competing interests: Hamutu Ojiyed reports financial support was provided by Dutch Research Council. Hamutu Ojiyed reports a relationship with Swiss Blue Energy that includes: funding grants.

Data availability

Data will be made available on request.

Acknowledgements

The authors would like to thank Anton Lefering, Bert Zwart, Robert

Dankelman and Michel Steenvoorden for their experimental assistance, Jouke Heringa and Karel Prokes for discussion about group theory and Anika Kiecana, Fengqi Zhang, Hanggai Wuliji for neutron diffraction refinement discussion. This work was financially supported by the Dutch Research Council with Project no. 680–91-013, Swiss Blue Energy and RSP Technology.

References

[1] C. Forman, I.K. Muritala, R. Pardemann, B. Meyer, Estimating the global waste heat potential, Renew. Sust. Energ. Rev. 57 (2016) 1568–1579.
[2] G. Schierning, Bring on the heat, Nat. Energy 3 (2018) 92–93.
[3] M. Araiz, Á. Casi, L. Catalán, Á. Martínez, D. Astrain, Prospects of wasteheat recovery from a real industry using thermoelectric generators: Economic and power output analysis, Energy Convers. Manag. 205 (2020) 112376.
[4] O.P. Dimitriev, Thermomechanical energy converters for harvesting thermal energy: a review, J. Renew. Mater. 11 (2023) 4.
[5] V. Srivastava, Y. Song, K. Bhatti, R.D. James, The direct conversion of heat to electricity using multiferroic alloys, Adv. Energy Mater. 1 (2011) 97–104.
[6] Y. Gao, W. Liu, S. Zhu, Thermoplastic polyolefin elastomer blends for multiple and reversible shape memory polymers, Ind. Eng. Chem. Res. 58 (42) (2019) 19495–19502.
[7] G.W. Swift, Thermoacoustic engines, J. Acoust. Soc. Am. 84 (4) (1988) 1145–1180.
[8] N. Tesla, Thermo-magnetic motor, U.S. patent 396121A (Jan. 15 1889).
[9] N. Tesla, Pyromagneto-electric generator, U.S. patent 428057A (May 13 1890).
[10] E. Brück, O. Tegus, X.W. Li, F.R. de Boer, K.H.J. Buschow, Magnetic refrigeration towards room-temperature applications, Phys. B 327 (2003) 431–437.
[11] O. Tegus, E. Brück, K.H.J. Buschow, F.R. de Boer, Transition-metal-based magnetic refrigerants for room-temperature applications, Nature 415 (2002) 150–151.
[12] A. Kitanovski, Energy applications of magnetocaloric materials, Adv. Energy Mater. 10 (2020) 1903741.
[13] T. Christiaanse, E. Brück, Proof-of-concept static thermomagnetic generator experimental device, Metall. Mater. Trans. E 1 (2013) 36–40.
[14] A. Waske, D. Dzekan, K. Sellschopp, D. Berger, A. Stork, K. Nielsch, S. Fähler, Energy harvesting near room temperature using a thermomagnetic generator with a pretzel-like magnetic flux topology, Nat. Energy 4 (2019) 68–74.
[15] V.K. Pecharsky, K.A. Gschneidner Jr., Giant magnetocaloric effect in $Gd_5(Si_2Ge_2)$, Phys. Rev. Lett. 78 (1997) 4494–4497.
[16] L. Morellon, J. Blasco, P.A. Algarabel, M.R. Ibarra, Nature of the first-order antiferromagnetic-ferromagnetic transition in the Ge-rich magnetocaloric compounds $Gd_5(Si_xGe_{1-x})_4$, Phys. Rev. B 62 (2000) 1022–1026.
[17] A.O. Pecharsky, K.A. Gschneidner Jr., V.K. Pecharsky, C.E. Schindler, The room temperature metastable/stable phase relationships in the pseudo-binary Gd_5Si_4-Gd_5Ge_4 system, J. Alloy. Comp. 338 (2002) 126–135.
[18] Y. Mozharivskyj, A.O. Pecharsky, V.K. Pecharsky, G.J. Miller, On the high-temperature phase transition of $Gd_5Si_2Ge_2$, J. Am. Chem. Soc. 127 (2005) 317–324.
[19] L. Morellon, P.A. Algarabel, M.R. Ibarra, J. Blasco, B. Garcia-Landa, Magnetic-field-induced structural phase transition in $Gd_5(Si_{1.8}Ge_{2.2})$, Phys. Rev. B 58 (1998) R14721–R14724.
[20] N.T. Trung, Z.Q. Ou, T.J. Gortenmulder, O. Tegus, K.H.J. Buschow, E. Brück, Tunable thermal hysteresis in MnFe(P,Ge) compounds, J. Appl. Phys. 99 (2006) 08Q107.
[21] H. Yibole, F. Guillou, Y.K. Huang, G.R. Blake, A.J.E. Lefering, N.H. van Dijk, E. Brück, First-order ferromagnetic transition in single-crystalline $(Mn,Fe)_2(P,Si)$, Appl. Phys. Lett. 107 (2015) 162403.
[22] Z.Q. Ou, L. Zhang, N.H. Dung, L. van Eijck, A.M. Mulders, M. Avdeev, N.H. van Dijk, E. Brück, Neutron diffraction study on the magnetic structure of Fe_2P-based $Mn_{0.66}Fe_{1.29}P_{1-x}Si_x$ melt-spun ribbons, J. Magn. Magn. Mater. 340 (2013) 80–85.
[23] X.F. Miao, L. Caron, J. Cedervall, P.C.M. Gubbens, P. Dalmas de Réotier, A. Yaouanc, F. Qian, A.R. Wildes, H. Luetkens, A. Amato, N.H. van Dijk, E. Brück, Short-range magnetic correlations and spin dynamics in the paramagnetic regime of $(Mn,Fe)_2(P,Si)$, Phys. Rev. B 94 (2016) 014426.
[24] F. Guillou, S. Liting, O. Haschuluu, Z.Q. Ou, E. Brück, O. Tegus, H. Yibole, Room temperature magnetic anisotropy in Fe_2P-type transition metal based alloys, J. Alloy. Comp. 800 (2019) 403–411.
[25] F.X. Hu, X.L. Qian, J.R. Sun, G.J. Wang, X.X. Zhang, Z.H. Cheng, B.G. Shen, Magnetic entropy change and its temperature variation in compounds $La(Fe_{1-x}Co_x)_{11.2}Si_{1.8}$, J. Appl. Phys. 92 (2002) 3620–3623.
[26] Y.F. Chen, F. Wang, B.G. Shen, F.X. Hu, J.R. Sun, G.J. Wang, Z.H. Cheng, Magnetic properties and magnetic entropy change of $LaFe_{11.5}Si_{1.5}H_y$ interstitial compounds, J. Phys.: Condens. Matter 15 (2003) L161–L167.
[27] S.A. Nikitin, G. Myalikgulyev, A.M. Tishin, M.P. Annaorazov, K.A. Asatryan, A. L. Tyurin, The magnetocaloric effect in $Fe_{49}Rh_{51}$ compound, Phys. Lett. A 148 (6-7) (1990) 363–366.
[28] M.P. Annaorazov, K.A. Asatryan, G. Myalikgulyev, S.A. Nikitin, A.M. Tishin, A. L. Tyurin, Alloys of the Fe-Rh system as a new class of working material for magnetic refrigerators, Cryogenics 32 (1992) 867–872.
[29] F.X. Hu, B.G. Shen, J.R. Sun, Magnetic entropy change in $Ni_{51.5}Mn_{22.7}Ga_{25.8}$ alloy, Appl. Phys. Lett. 76 (2000) 3460–3462.
[30] M. Pasquale, C.P. Sasso, L.H. Lewis, L. Giudici, T. Lograsso, D. Schlagel, Magnetostructural transition and magnetocaloric effect in $Ni_{55}Mn_{20}Ga_{25}$ single crystals, Phys. Rev. B 72 (2005) 094435.
[31] J. Marcos, L. Mañosa, A. Planes, Multiscale origin of the magnetocaloric effect in Ni-Mn-Ga shape-memory alloys, Phys. Rev. B 68 (2003) 094401.
[32] B. Aronsson, G. Lundgren, X-Ray investigations on Me-Si-B System I, Acta Chem. Scand. 13 (1959) 433–441.
[33] B. Aronsson, I. Engström, X-Ray investigations on Me-Si-B System II, Acta Chem. Scand. 14 (1960) 1403–1413.
[34] S. Rundqvist, X-Ray investigations of the ternary system Fe-P-B. Some feature of the systems Cr-P-B, Mn-P-B, Co-P-B and Ni-P-B, Acta Chem. Scand. 16 (1962) 1–19.
[35] R. Wäppling, T. Ericsson, L. Häggström, Y. Andersson, Magnetic properties of Fe_5SiB_2 and related compounds, J. Phys. Colloq. C6 (1976) 591–593.
[36] L. Häggström, R. Wäppling, T. Ericsson, Mössbauer and X-ray studies of Fe_5PB_2, J. Solid State Chem. 13 (1976) 84–91.
[37] D.M. de Almeida, C. Bormio-Nunes, C.A. Nunes, A.A. Coelho, G.C. Coelho, Magnetic characterization of Mn_5SiB_2 and Mn_5Si_3 phases, J. Magn. Magn. Mater. 321 (2009) 2578–2581.
[38] Z.G. Xie, D.Y. Geng, Z.D. Zhang, Reversible room-temperature magnetocaloric effect in Mn_5PB_2, Appl. Phys. Lett. 97 (2010) 202504.
[39] M.A. McGuire, D.S. Parker, Magnetic and structural properties of ferromagnetic Fe_5PB_2 and Fe_5SiB_2 and effects of Co and Mn substitutions, J. Appl. Phys. 118 (2015) 163903.
[40] M. Werwiński, Magnetic properties of Fe_5SiB_2 and its alloys with P, S, and Co, Phys. Rev. B 93 (2016) 174412.
[41] D. Hedlund, J. Cedervall, A. Edström, M. Werwiński, S. Kontos, O. Eriksson, J. Rusz, P. Svedlindh, M. Sahlberg, K. Gunnarsson, Magnetic properties of the Fe_5SiB_2–Fe_5PB_2 system, Phys. Rev. B 96 (2017) 094433.
[42] M. Werwiński, Magnetocrystalline anisotropy of Fe_5PB_2 and its alloys with Co and 5*d* elements: a combined first-principles and experimental study, Phys. Rev. B 98 (2018) 214431.
[43] J. Cedervall, E. Nonnet, D. Hedlund, L. Häggström, T. Ericsson, M. Werwiński, A. Edström, J. Rusz, P. Svedlindh, K. Gunnarsson, M. Sahlberg, Influence of cobalt substitution on the magnetic properties of Fe_5PB_2, Inorg. Chem. 57 (2018) 777–784.
[44] J. Thakur, P. Rani, M. Tomar, V. Gupta, H.S. Saini, M.K. Kashyap, Tailoring in-plane magnetocrystalline anisotropy of Fe_5SiB_2 with Cr-substitution, AIP Conf. Proc. 2115 (2019) 030506.
[45] T. Ericsson, L. Häggström, R. Wäppling, Spin rotation in Fe_5SiB_2, Phys. Scr. 17 (1978) 83–86.
[46] J. Cedervall, S. Kontos, T.C. Hansen, O. Balmes, F.J. Martinez-Casado, Z. Matej, P. Beran, P. Svedlindh, K. Gunnarsson, M. Sahlberg, Magnetostructural transition in Fe_5SiB_2 observed with neutron diffraction, J. Solid State Chem. 235 (2016) 113–118.
[47] L. van Eijck, L.D. Cussen, G.J. Sykora, E.M. Schooneveld, N.J. Rhodes, A.A. van Well, C. Pappas, Design and performance of a novel neutron powder diffractometer: PEARL at TU Delft, J. Appl. Cryst. 49 (2016) 1398–1401.
[48] H.M. Rietveld, A profile refinement method for nuclear and magnetic structures, J. Appl. Cryst. 2 (1969) 65–71.
[49] J. Rodriguez-Carvajal, Recent advances in magnetic-structure determination by neutron powder diffraction, Phys. B 192 (1993) 55–69.
[50] J.R. de Laeter, J.K. Böhlke, P. de Bièvre, H. Hidaka, H.S. Peiser, K.J.R. Rosman, P. D.P. Tayler, Atomic weights of the elements: Review 2000 (IUPAC Technical Report), Pure Appl. Chem. 75 (2003) 683–800.
[51] K. Lefmann, Neutron Scattering: Theory, Instrumentation, and Simulation, Niels Bohr Institute, University of Copenhagen, 2007.
[52] D. Dzekan, A. Waske, K. Nielsch, S. Fähler, Efficient and affordable thermomagnetic materials for harvesting low grade waste heat, APL Mater. 9 (2021) 011105.
[53] V.K. Pecharsky, K.A. Gschneidner, Some common misconceptions concerning magnetic refrigerant materials, J. Appl. Phys. 90 (2001) 4614.
[54] J.Y. Law, V. Franco, L.M. Moreno-Ramírez, A. Conde, D.Y. Karpenkov, I. Radulov, K.P. Skokov, O. Gutfleisch, A quantitative criterion for determining the order of magnetic phase transitions using the magnetocaloric effect, Nat. Comm. 9 (2018) 2680.
[55] C.P. Bean, D.S. Rodbell, Magnetic disorder as a first-order phase transformation, Phys. Rev. 126 (1962) 104–115.
[56] N.H. van Dijk, Landau model evaluation of the magnetic entropy change in magnetocaloric materials, J. Magn. Magn. Mater. 529 (2021) 167871.
[57] L.D. Landau, On the theory of phase transitions. I, Zh. Eksp. Teor. Fiz. 7 (1937) 19–32.
[58] Y.Z. Song, N. Shi, S.Q. Deng, X.R. Xing, J. Chen, Negative thermal expansion in magnetic materials, Prog. Mater. Sci. 121 (2021) 100835.
[59] Y. Song, Q. Sun, M. Xu, J. Zhang, Y. Hao, Y. Qiao, S. Zhang, Q. Huang, X. Xing, J. Chen, Negative thermal expansion in $(Sc,Ti)Fe_2$ induced by an unconventional magnetovolume effect, Mater. Horiz. 7 (2020) 275–281.
[60] A.S. Wills, A new protocol for the determination of magnetic structures using simulated annealing and representational analysis (SARAh), Phys. B 276-278 (2000) 680–681.